Quantifying the impact of sulfate geoengineering on mortality from air quality and UV-B exposure

Sebastian D. Eastham[a],[*], Debra K. Weisenstein[b], David W. Keith[b], Steven R.H. Barrett[a]

[a] Laboratory for Aviation and the Environment, Department of Aeronautics and Astronautics, Massachusetts Institute of Technology, Cambridge, MA 02139, United States
[b] School of Engineering and Applied Sciences, Harvard University, Cambridge, MA 02139, United States

ABSTRACT

Sulfate geoengineering is a proposed method to partially counteract the global radiative forcing from accumulated greenhouse gases, potentially mitigating some impacts of climate change. While likely to be effective in slowing increases in average temperatures and extreme precipitation, there are known side-effects and potential unintended consequences which have not been quantified. One such consequence is the direct human health impact. Given the significant uncertainties, we take a sensitivity approach to explore the mechanisms and range of potential impacts. Using a chemistry-transport model, we quantify the steady-state response of three public health risks to 1 °C global mean surface cooling. We separate impacts into those which are "radiative forcing-driven", associated with climate change "reversal" through modification of global radiative forcing, and those "direct impacts" associated uniquely with using sulfate geoengineering to achieve this. We find that the direct (non-radiative forcing driven) impact is a decrease in global mortality of ~13,000 annually. Here the benefits of reduced ozone exposure exceed increases in mortality due to UV and particulate matter, as each unit of injected sulfur incurs 1/25th the particulate matter exposure of a unit of sulfur emitted from surface sources. This reduction is exceeded by radiative forcing-driven health impacts resulting from using sulfate geoengineering to offset 1 °C of surface temperature rise. Increased particulate matter formation at these lower temperatures results in ~39,000 mortalities which would have been avoided at higher temperatures. As such we estimate that sulfate geoengineering in 2040 would cause ~26,000 (95% interval: −30,000 to +79,000) early deaths annually relative to the same year without geoengineering, largely due to the loss of health benefits associated with CO_2-induced warming. These results account only for impacts due to changes in air quality and UV-B flux. They do not account for non-mortality impacts or changes in atmospheric dynamics, and must be considered in the wider context of other climate change impacts such as heatwave frequency and sea level rise.

1. Introduction

Sulfate geoengineering is one of several possible forms of solar radiation management (SRM), proposed as a method to reduce the net harm resulting from anthropogenic climate change. By promoting the formation of a long-lived stratospheric aerosol layer, a fraction of incoming solar radiation can be scattered back to space before it could be absorbed by the atmosphere, partially offsetting the net anthropogenic radiative forcing. The efficacy of a natural or artificial sulfate layer in reducing global temperature and precipitation has been widely investigated. Early investigations focused on large volcanic eruptions, which are known to produce transient stratospheric aerosol layers (McCormick et al., 1995), while later climate modeling studies explored the possible outcomes of sulfate geoengineering (Rasch et al., 2008). Although the climate and public health impacts of sulfate

geoengineering have been discussed (NAS, 1992; Pitari et al., 2014; Effiong and Neitzel, 2016), to date there has not been a quantitative evaluation of how global mortality rates might be affected by changes in air quality or UV-B exposure resulting from such a strategy.

Air quality, specifically surface-level concentrations of ozone and fine particulate matter ($PM_{2.5}$), has been linked quantitatively to changes in mortality rates through exposure response functions based on epidemiological studies (Hoek et al., 2013; Jerrett et al., 2009). A similar function has been developed for exposure to UV-B radiation, with the aim of estimating avoided skin cancer incidence due to implementation of the Montreal protocol (Slaper et al., 1996). The existence of these functions allows the effect of any policy or technology on each of these factors to be calculated and compared in common units. Degraded air quality is estimated to cause ~8% of all global mortality in 2015 (Cohen et al., 2017), and changes to air quality are
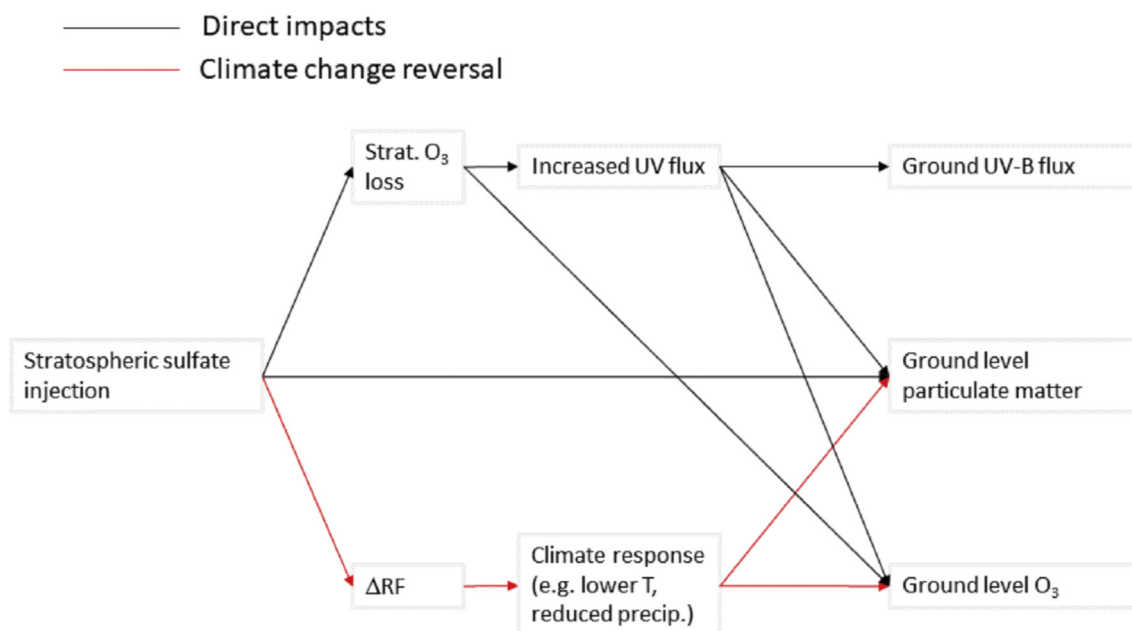
Fig. 1. Influence diagram for impacts of sulfate geoengineering on public health. Only first-order influences are shown here. Minor contributions which may still be significant, such as the direct scattering effect of sulfate aerosols on surface UV-B flux, are not shown for the sake of clarity.

frequently considered in the context of climate change. A recent study found that mitigation of greenhouse gas emissions from an "unconstrained" scenario down to those in the IPCC RCP4.5 scenario would result in ~1.3 million fewer mortalities per year in 2050 due to both changes in climate and the required changes in emissions (West et al., 2013). This estimation technique has been applied in source-specific impacts evaluations such as for aircraft emissions (e.g. Eastham and Barrett, 2016), but has not yet been applied to an analysis of sulfate geoengineering.

The mechanisms by which an SRM proposal affects these outcomes can be separated into two categories: the "direct" impacts of the method, and the "RF (radiative-forcing)-driven" impacts. Fig. 1 gives a conceptual overview of how these categories apply to the impact pathways between stratospheric injection of sulfate aerosol and human health impacts. "Direct impacts", shown in black, include any effects of the technique which would occur even if there were no effect on the climate. For sulfate geoengineering, an example would be the descent of injected aerosol to the surface. Falling aerosol will add to the existing burden of near-surface fine particulate matter, degrading surface air quality and incurring public health damages in the form of increased respiratory disease mortality rates. This impact would occur regardless of whether the injected aerosol successfully reduced the net radiative imbalance. A second example is the effect of sulfate geoengineering on stratospheric ozone, and the resulting effect on the intensity of surface-level UV-B radiation. Although this has been discussed in the literature in terms of changes in mean intensity (Pitari et al., 2014; Nowack et al., 2016; Xia et al., 2017), the impact on human health has never been quantified.

"RF-driven" impacts, shown in Fig. 1 in red, include only those which result from the change in radiative forcing achieved by the injected aerosol. Although there are some ways in which the effects of sulfate geoengineering are expected to differ from a simple reversal of climate change (Caldeira et al., 2013), RF-driven impacts are likely to be dominated by the avoided effects of climate change. For example, increasing temperatures associated with climate change are expected to increase ozone concentrations in polluted regions (Fiore et al., 2012). By mitigating future increases in temperature, sulfate geoengineering might reduce total mortality due to ozone exposure relative to the avoided future scenario. Similarly, any potential localized benefits of

climate change such as increased crop yields in previously-unproductive regions (Reilly et al., 1994) would also be lost.

The relative contribution of each impact pathway to the total impact of sulfate geoengineering depends on multiple uncertain quantities. Although volcanic events have provided evidence that a stratospheric sulfate layer can provide a negative radiative forcing, the total forcing achieved per unit mass injected varies between studies. For a given target outcome – for example, a 1 °C reduction in global average surface temperature – the required rate of sulfate injection will depend on the lifetime and properties of the aerosol layer produced, in addition to the sensitivity of the climate to an increase in stratospheric aerosol optical depth. There are large differences in the estimates of the RF per unit sulfate, differences that depend, in part, on the way sulfates are introduced to the stratosphere (Pierce et al., 2010; Niemeier and Timmreck, 2015). The magnitude of these variables could affect the total impact of sulfate geoengineering, and the contribution of each pathway. Lower RF per unit sulfate means larger direct impacts per unit climate benefit. A world with a low climate sensitivity (the rate of change of temperature with respect to aerosol optical depth, $\partial T / \partial \tau$) will require more injected mass to achieve the same temperature reduction target than a world with a high climate sensitivity, but the amount of temperature reduction used in a low-sensitivity world will presumably be correspondingly less. Although temperature-related impacts would be unaffected, impacts directly related to the presence of more stratospheric aerosol, including stratospheric ozone changes, and therefore UV-B exposure, will be greater for the former case than the latter. Although a spot estimate of geoengineering's impacts on global mortality can be achieved in a single model run, a more nuanced approach is required to understand what the contribution of each pathway is to the total, and how these contributions are affected by uncertainty in input parameters such as climate sensitivity.

We use a global chemistry-transport model (CTM) to compute the response of air quality and population UV-B exposure to sulfate geoengineering at a rate of 1 TgS/yr, isolating the direct and RF-driven impacts using a hybrid modeling approach. Direct impacts of sulfate geoengineering are estimated using offline CTM simulations, in which meteorological fields are specified and no climate response is simulated. RF-driven impacts are estimated by re-running the CTM with perturbed meteorological fields, using a GCM to calculate temperature

Table 1
Simulation parameters used for each GEOS-Chem model run.

Simulation	Sulfate injection	Precipitation adjustment	Temperature adjustment	Chemistry
Baseline (B)	–	–	–	Yes
Calibration (0)	Yes	–	–	Yes
Central (C)	Yes	Yes	Yes	Yes
Precipitation sensitivity (S_P)	Yes	–	Yes	Yes
Temperature sensitivity (S_T)	Yes	Yes	–	Yes
Inert aerosol (I)	Yes	–	–	–

relative change in the global average precipitation rate. In both cases, seasonal variation is captured by using monthly mean values rather than an annual average. Further information is provided in the SI.

2.2. Calculation of impacts for a fixed injection rate

As described at the start of section 2, we first calculate the total impact of sulfate injection at a rate of 1 TgS/yr, and separate these impacts into direct and RF-driven pathways. To achieve this, we run 6 separate GEOS-Chem simulations, shown in Table 1.

The net impact of 1 TgS/yr of sulfate geoengineering on air quality and UV-B exposure is estimated by subtracting the results of the baseline simulation (B) from those of the central simulation (C). The exposure resulting from all emissions in a given scenario (e.g. scenario S) can be represented as E(S), such that the change in exposure due to all effects combined is E(C) – E(B). In the central simulation, all impact pathways are simulated together. 1 TgS/yr of aerosol is injected. Air temperatures are decreased relative to the baseline simulation according to the pre-calculated temperature sensitivity field described in section 1.1, scaled by the 0.079 stratospheric AOD estimated from the calibration simulation. Global precipitation is also decreased relative to the baseline. Post-simulation analysis of the simulation C showed a stratospheric AOD increase of 0.075, within 6% of the value used for calibration.

The contribution of direct (non-RF) pathways to the total impact of sulfate geoengineering is estimated using results from the calibration simulation (0). Specifically, the total contribution of direct pathways (all black arrows in Fig. 1) to the net impact of sulfate geoengineering on air quality and UV-B exposure is calculated by subtracting the "RF-driven" impact from the total impact, as [E(C) – E(B)] – [E(C) – E(0)]. This is equivalent to E(0) – E(B) and does not account for second-order terms resulting from, for example, the effect of changes in precipitation on the direct pathways. However, these terms are quantified in Appendix B and found to be negligible.

The contribution of each of the RF-driven pathways to the total is isolated by performing two sensitivity simulations. Each is identical to simulation C, but without one of the two climate perturbations. For example, in simulation S_T, sulfate aerosol is injected and global precipitation is reduced, but temperatures are left unperturbed relative to the baseline. The difference in air quality and UV-B impacts between simulation S_T and simulation C, calculated as (for example) E(C) – E(S_T), provides an estimate of the contribution of temperature change (an RF-driven impact) to the net impact of sulfate geoengineering. We refer to the contribution of each of the two RF-driven pathways as the "offset warming" and "offset precipitation" impacts, on the basis that these changes are offsetting impacts of climate change. These pathways account for the effect that the geoengineering-attributable change in RF, and therefore the change in climate, has on background air quality and UV-B exposure. Again, cross terms resulting from interaction between temperature- and precipitation-driven impacts are quantified in Appendix B and found to be negligible.

We run one additional simulation to better disaggregate the direct (non-RF-driven) pathways. The contribution of descending injected sulfate aerosol to concentrations of fine particulate matter at the surface is calculated by performing a separate simulation, without temperature or precipitation perturbations, in which a chemically unreactive aerosol is injected (simulation I). This aerosol undergoes the same loss mechanisms as sulfate aerosol. This direct impact pathway is referred to as the "descending aerosol" pathway. The net impact due to descending aerosol is simply E(I), as no other aerosol emissions or formation pathways are included in this simulation.

Any changes in air quality and UV-B exposure observed in simulation 0 which are not present in this inert simulation are assumed to be the photochemical response of the atmosphere to the increased stratospheric loading, calculated as [E(0) – E(B)] – E(I). This direct impact pathway is referred to as the "photochemical" pathway. Specifically, this is the contribution of photochemical processes to the total impact of sulfate geoengineering after the impacts of RF changes on background air quality and UV-B exposure have been accounted for.

2.3. Impacts and uncertainty quantification for a fixed target warming offset

The combination of simulations listed in Table 1 provides an estimate of how sulfate geoengineering at a rate of 1 TgS/yr would impact air quality and UV-B exposure, in addition to the contribution from each of four direct and RF-driven pathways. Based on the mean climate sensitivity from CanESM2 and the calculated stratospheric AOD from GEOS-Chem, this is also the impact of sulfate geoengineering sufficient to offset 1 °C of warming. By assuming linearity in the atmospheric response, these same results can be used to answer a different question: the contribution of uncertainty in the atmospheric response to both the total impact and the contributions of each pathway.

We use a Monte-Carlo approach to explore how uncertainty in three climate variables (Table 2) affects the total calculated change in air quality and UV-B exposure, holding constant the target of offsetting 1 °C of surface warming. We assume a linear relationship for each of the following pairs of variables, with the slope of each relationship treated as an uncertain variable: between injection rate and stratospheric aerosol burden (the aerosol lifetime); between stratospheric AOD and temperature change (the climate sensitivity); and between temperature change and precipitation change (the hydrological sensitivity). In each Monte-Carlo simulation, an independent draw of these three variables is taken, and the total impact is recalculated by re-weighting the

Table 2
Uncertain parameters applied in Monte-Carlo simulations when converting simulation output to mortality estimates. Triangular distributions are shown as the mode and 95% bounds. Limits of the distribution consistent with the 95% bounds were calculated at simulation time. The "discrete" distribution corresponds to random selection of one of the listed values, taken from the results of 4 models running the GeoMIP G4 simulations. *T* denotes temperatures; τ denotes stratospheric AOD; *P* denotes global mean precipitation rate; *M* denotes number of premature mortalities; χ denotes population-weighted concentration.

Parameter	Distribution
Global temperature sensitivity ($\partial T/\partial \tau$) (K)	Discrete [-7.2, −7.3, −12, −19]
Global hydrological sensitivity ($\partial P/\partial T$) (% K^{-1})	Discrete [1.7, 2.4, 2.6, 2.9]
Mean stratospheric aerosol lifetime (years)	Uniform [1.0–2.4]
Ozone health response ($dM/d\chi$) (% $ppbv^{-1}$)	Triangular [0.100–0.104 – 0.107]
$PM_{2.5}$ health response ($dM/d\chi$) (% ($\mu g\ m^{-3}$)$^{-1}$)	Triangular [0.500–1.10 – 1.60]
UV-B health response dose factor (unitless)	Triangular [0.2–0.6 – 1.0]

contribution from each of the four pathways.

We assume that a reduction in the hydrological sensitivity will result in a proportional reduction in impacts due to the RF-driven "offset precipitation" pathway. We assume that a reduction in the climate sensitivity will result in a proportional increase in impacts due to the direct impacts, on the assumption that a decreased climate sensitivity implies an increased AOD for the same warming target, and therefore an increased injection rate. Finally, we assume that a decreased aerosol lifetime implies an increase in the direct "descending aerosol" pathway only. This is on the basis that decreased aerosol lifetimes imply an increased injection rate, but the same overall AOD, with no effect on the overall RF achieved.

In each uncertain draw, aerosol lifetime is chosen based on a uniform distribution between 1 and 2.4 years. This range spans most published estimates (Heckendorn et al., 2009; Pierce et al., 2010; Rasch et al., 2008) and includes the lifetime of 2.4 years simulated by GEOS-Chem in the calibration scenario. For the climate and hydrological sensitivity parameters, a value is randomly chosen from a set of four GeoMIP experiment G4 simulations with different climate models (CanESM2, MIROC-ESM-CHEM, BNU-ESM and GISS-ER-2) (Kravitz et al., 2013). The parameter distributions are shown in detail in Table 2.

This process is described in more detail in the SI, and an assessment of the accuracy of the linearity assumption is performed in Appendices A and Appendices B. Changes in second order effects such as climate variability and atmospheric dynamics, which may affect cross-tropopause mass flux and surface-level stagnation, are not modeled but are a clear priority for future work.

One potentially significant feedback which is not considered here is the effect of sulfate geoengineering on cloud formation and properties. The increase in cloud condensation nuclei (CCN) and ice nuclei resulting from the descent of emitted fine aerosol into the upper troposphere could result in increased cirrus cloud formation, an effect which by one estimate could contribute up to 60% of the net radiative forcing due to sulfate geoengineering (Kuebbeler et al., 2012). It is also possible that warm cloud formation could be affected by the increase in CCN. Although this is not likely to be significant for this study, in which the maximum injection rate considered is ~5–10% of current anthropogenic sulfur emissions (Smith et al., 2011), scenarios involving higher rates of sulfate geoengineering emissions could result in additional changes to precipitation patterns, intensity, and frequency which could significantly affect surface concentrations of $PM_{2.5}$. Changes in cloud cover would also affect surface UV-B intensity, potentially mitigating the skin cancer damages simulated here.

2.4. Calculation of health impacts

Once the total change in air quality and UV-B exposure for a given uncertain draw has been computed, we convert the simulated changes in population exposure into an estimate of global mortality. The gradients of the exposure response functions (ERFs), which reflect the sensitivity of health outcomes to population exposure, are treated as uncertain variables, with distributions described in Table 2. We use the non-linear Jerrett et al. (2009), Hoek et al. (2013) and Slaper et al. (1996) ERFs for ozone, $PM_{2.5}$ and UV-B exposure respectively. The Hoek ERF was chosen for $PM_{2.5}$ over the more common Krewski et al. (2009) ERF as it is a global meta-analysis of epidemiological studies including Asia, whereas the latter is an in-depth epidemiological study of the USA only. The effect of applying widely-used alternative ERFs for $PM_{2.5}$ such as those of Krewski or Burnett et al. (2014) is quantified, as is the effect of applying concentration thresholds for both $PM_{2.5}$ and ozone.

One thousand draws are performed for all six uncertain variables, using the Sobol pseudo-random sampling sequence to improve convergence. Sensitivity of the results to each input is calculated using the first-order contributions to total variance. This provides an estimate of the first-order sensitivity indices (Sobol indices), corresponding to the

fractional contributions of uncertainty in each input to the total variance in the output (Saltelli et al., 2008).

Two additional scenarios are simulated with alternative assumptions. The first applies region-specific factors to precipitation changes to quantify the relative importance of global and regional precipitation changes in calculating mortality. The second models a hypothetical low-halogen future to account for the relative contributions of anthropogenic halogens in sulfate geoengineering impact calculations (Tilmes et al., 2009, 2012; Heckendorn et al., 2009). A full description of the approach used for these simulations is given in the SI.

3. Results

Impacts of implementing sulfate geoengineering sufficient to offset 1 °C of surface warming in 2040 are presented below. Direct pathways are discussed first, followed by RF-driven pathways. A summary of the total impacts is provided in the Discussion section. In each case, the calculated change in mortality is the result of the full Monte-Carlo simulation, propagating uncertainty in climate sensitivity, aerosol microphysics, and exposure response. All impacts are calculated for a projected global population in 2040 of 9 billion people (United Nations, 2013).

3.1. Direct impacts

The first of the direct impacts considered is the descent of injected aerosol to the surface, increasing the surface-level concentration of $PM_{2.5}$. We find that this pathway results in an additional 7400 premature mortalities per year due to degraded air quality (95% interval: 2300 to 16,000). This implies that injection of aerosol into the stratosphere sufficient to offset 1 °C of surface warming would result in a net increase in mortality of the same order of magnitude as attributable to jet fuel sulfur in 2006 (Barrett et al., 2012), and an order of magnitude lower than the impacts attributable to shipping in 2002 (Corbett et al., 2007). In an additional sensitivity simulation, we simulated continuous emission of an equal mass of aerosol at the surface, distributed according to present-day surface-level sulfur emitters. Per unit mass emitted, we find that surface-level emissions of sulfate result in 25 times greater population exposure to $PM_{2.5}$ than results from emitting the same aerosol into the stratosphere, while achieving a greater radiative forcing offset due to the longer lifetime of stratospheric aerosol.

Direct photochemical changes, excluding the impact of injected aerosol descending to the surface, is net negative, with a mean outcome of −42,000 premature mortalities per year (95% interval: −42,000 to −4900). This response is dominated by decreased ozone exposure at the surface. Enhanced stratospheric ozone depletion results in reduced ozone mixing ratios in surface-bound stratospheric air masses, while the increased mid-tropospheric flux of UV radiation reduces the photochemical steady-state concentration of ozone throughout the troposphere (Zhang et al., 2014). Changes in the atmospheric dynamics, including the stratosphere-troposphere ozone exchange rate due to dynamical effects of sulfate geoengineering, are not considered but may affect this result (Kirtman et al., 2014). The mean change in global mortality due to reduced ozone exposure in this pathway is −23,000, exceeding the mean increase in skin cancer mortality of 4100 due to increased UV-B exposure. The reduction in ozone also prompts a small decrease in $PM_{2.5}$, resulting in −1400 premature mortalities (−2400 to −520) per year. This suggests that a small depletion in stratospheric ozone may result in a net reduction in global mortality. This is a surprising result, and implies that future increases in stratospheric ozone such as those projected under some climate change scenarios (Li et al., 2009) might be considered as a public health threat. However, this outcome may be specific to the circumstances of the stratospheric ozone loss, and warrants further research.

Previous studies have shown that the stratospheric ozone loss due to sulfate geoengineering is sensitive to the assumed halogen loading, with

one study even finding a reversal of sign (Tilmes et al., 2009, 2012; Heckendorn et al., 2009). We simulate an alternative scenario which corresponds to the theoretical minimum atmospheric halogen loading. In this scenario all anthropogenic halogen emissions are set to zero, as are the initial concentrations for all long-lived anthropogenic halogen gases (see SI for details). We find that total ozone column depletion is reduced by 31% relative to the scenario with RCP 4.5 halogen emissions, resulting in 2500 fewer premature mortalities due to skin cancer, and 4800 fewer due to $PM_{2.5}$ exposure. These benefits are exceeded by the increased ozone exposure in this scenario, resulting in 7600 additional mortalities. The net result is that the reduction in global mortality due to direct photochemical impacts alone is smaller in magnitude by 3.6% under a low-halogen scenario, relative to the baseline scenario. This again suggests that a relative increase in ozone concentrations may have a net public health disbenefit, considering only air quality and UV-B exposure.

Considering only direct impact pathways, sulfate geoengineering sufficient to offset 1 °C of surface warming results in a net benefit, with a global change of −13,000 premature mortalities per year (sum of central estimates). Although we find 7400 (2300 to 16,000) additional premature mortalities due to direct population exposure to injected aerosol, this is counteracted by −20,000 (−42,000 to −4900) premature mortalities due to photochemical impacts resulting from the increased sulfur loading of the stratospheric aerosol layer.

3.2. RF-driven impacts

The calculated RF-driven impacts of sulfate geoengineering on air quality are consistent with prior literature examining the related problem of the response of air quality to CO_2-driven warming. Reduced temperatures relative to the projected future scenario result in enhanced partitioning of HNO_3 from background emissions into nitrate aerosol, and therefore an increase in surface $PM_{2.5}$. We find that this dominates other $PM_{2.5}$ formation mechanisms which reduce in response to cooler surface temperatures, such as production of biogenic aerosols. The result is that, by offsetting 1 °C of surface warming from climate change, sulfate geoengineering results in an additional 69,000 premature mortalities annually (41,000 to 95,000). This increase is

accompanied by a significant decrease in premature mortality due to the avoided effect of global warming on ozone. Ozone concentrations in polluted regions decrease with temperature as photochemical production is slowed, such that sulfate geoengineering results in −43,000 (−67,000 to −19,000) premature mortalities per year due to ozone exposure relative to the avoided future. The effect of temperature change on UV-B exposure is negligible.

The other RF-driven impact of sulfate geoengineering is lower overall precipitation rates, offsetting some of the increased precipitation projected to result from climate change. Decreased precipitation results in longer lifetimes for $PM_{2.5}$ and therefore in increased $PM_{2.5}$ exposure globally. The total RF-driven impact of changes in precipitation from sulfate geoengineering is an additional 14,000 (7100 to 21,000) premature mortalities per year, with negligible effects on ozone and UV-B exposure.

This approach assumes that precipitation will be uniformly affected across all locations, and all aggregated impacts in the following sections are calculated on this assumption. However, sulfate geoengineering is likely to reduce precipitation by a greater proportion in some regions than in others (Kravitz et al., 2014). We run an additional, sensitivity simulation in which precipitation rate modifications are derived and applied on a local basis rather than a global basis, using a separate factor derived from the GeoMIP G4 CanESM2 simulation for each of 21 climatologically-distinct regions (see SI for details). In this scenario, the impacts of precipitation are increased by 15%. The increase occurs almost exclusively in Asia and Eastern Europe. Here the relative reduction in precipitation is 1.5 and 4.5 times the global average, respectively, resulting in longer lifetimes for $PM_{2.5}$ as washout is decreased. However, whether using global or regional precipitation adjustments, impacts due to temperature change remain dominant factor in RF-driven mortality impact pathways of sulfate geoengineering.

The net effect of RF-driven impact pathways on global air-quality and UV-B exposure is a net increase in mortality, reflecting the loss of climate change-driven air quality benefits associated with increasing temperature and precipitation. We find a combined central estimate of 39,000 additional mortalities per year due to this offsetting. This total is made up of +26,000 (−12,000 to +63,000) premature mortalities due to avoided temperature change, and +13,000 (+6600 to +20,000)
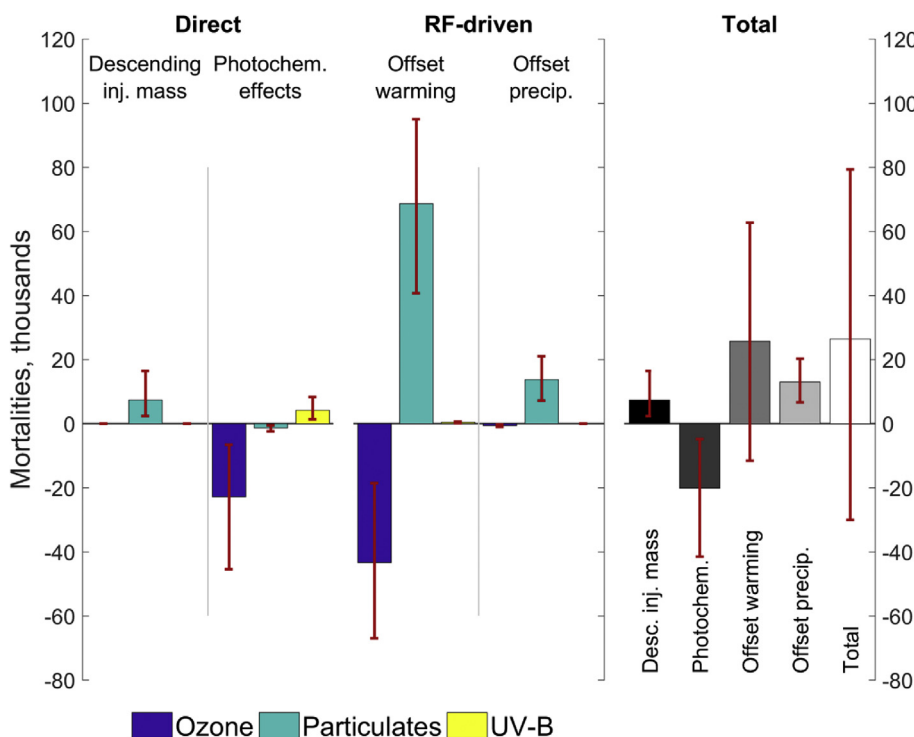

Fig. 2. Annual premature mortality impacts resulting from sulfate geoengineering sufficient to offset 1 °C of surface warming. Impacts are separated by pathway, based on Fig. 1, and by exposure type. The left panel shows the contributions to each pathway's total impact, separated by exposure type. The right hand subplot shows how each impact pathway contributes to the total. "Descending inj. mass" corresponds to direct exposure of the population to injected aerosol mass as it descends to the surface. "Photochem. effects" corresponds to photochemical changes resulting from the increased aerosol optical depth and surface area, including induced changes in stratospheric ozone columns. "Offset warming" corresponds to temperature change, "Offset precip." to reductions in precipitation. Solid bars show the mean value of Monte Carlo simulation outcomes (n = 1000). Error bars show the 2.5 and 97.5th percentile values.

due to precipitation reduction.

These results are sensitive to the modeled impact of climate change on surface air quality. We find that, for both RF-driven pathways, sulfate geoengineering offsets climate change-related increases in ozone and decreases in $PM_{2.5}$, with the magnitude of mortality impacts from the latter change exceeding those from the former. While increases of ozone under climate change are widely reported in the literature, the sign of the impact of climate change on surface $PM_{2.5}$ concentrations is uncertain (Fiore et al., 2012). The net outcome of RF-driven impacts is likely to change as our understanding of the impacts of climate change is further refined.

4. Discussion

In total, and considering only the effects on air quality and UV-B exposure, sulfate geoengineering sufficient to offset 1 °C of warming results in +26,000 premature mortalities annually (95% confidence interval of −30,000 to +79,000). Fig. 2 shows a graphical breakdown of incurred mortalities by pathway and by exposure type, with numerical values shown in Table 3. This total is made up of 39,000 additional mortalities due to RF-driven pathways, partially offset by 26,000 prevented mortalities due to direct pathways, as outlined in Fig. 1. In 17% of cases, mortality reductions due to decreased ozone exposure exceed the combined global mortality impacts of increased $PM_{2.5}$ and UV-B exposure, resulting in a net decrease in global mortality due to sulfate geoengineering. Overall, surface air quality and skin cancer impacts are dominated by increases in mortality due to RF-driven pathways, whereas the direct impact pathways of sulfate geoengineering are net beneficial by these metrics.

For all four atmospheric mechanisms, mortality due to surface ozone exposure is consistently decreased by sulfate geoengineering, whereas mortality due to $PM_{2.5}$ exposure varies in sign. Increases in nitrate aerosol due to reduced surface warming result, on average, in greater health impacts than the benefits associated with reduced ozone. UV-B exposure is only significantly affected by direct photochemical effects of sulfate geoengineering, but the contribution of changes in UV-B exposure to the overall impact of sulfate geoengineering is an order of magnitude smaller than the contributions of changes in ozone or $PM_{2.5}$ exposure.

When considering only the direct photochemical consequences of sulfate geoengineering, the total skin cancer mortality increase is exceeded by the ozone mortality decrease in all uncertain variable draws. This counterintuitively implies that limited stratospheric ozone destruction may be of net benefit in terms of premature mortality and human lifespan, and that reduction of anthropogenic halogen emissions may increase rather than reduce health impacts due to sulfate geoengineering. However, this does not take into account non-mortality outcomes of exposure to UV-B such as cataract formation and non-melanoma skin cancer, which is less fatal but several orders of magnitude more common than melanoma skin cancer (Guy et al., 2015;

Slaper et al., 1996).

Uncertainty in the ERFs for $PM_{2.5}$ and ozone have the greatest first-order effect on overall variance in the global mortality impact of sulfate geoengineering, contributing 44% and 50% of the total variance in the result based on the calculated sensitivity indices. The first-order effects of uncertainty in climate response are an order of magnitude smaller, with the greatest contribution being 2.5% for temperature sensitivity with respect to optical depth. Uncertainty in the UV-B exposure response function, sensitivity of precipitation to temperature and uncertainty in aerosol lifetime each contribute 1% or less to overall uncertainty in the result. When calculating mortality due to $PM_{2.5}$ and ozone individually, ERF uncertainty remains the greatest contributor to overall variance, followed by uncertainty in the temperature sensitivity to optical depth. However, this ordering is reversed for mortalities due to UV-B exposure. Furthermore, application of an alternative ERF developed for global studies by Burnett et al. (2014) results in mortality due to geoengineering-attributable $PM_{2.5}$ falling by 22%. Mortalities calculated using several other ERFs are shown in the SI.

All simulations were performed at a relatively coarse horizontal resolution (4° × 5°). A 2013 study indicated that while surface ozone exposure is insensitive to grid resolution, use of coarse horizontal resolution when calculating outcomes could result in mortality due to $PM_{2.5}$ exposure being biased low by 30–40%. This is due to the covariance of peaks in $PM_{2.5}$ concentration and population centers, which is not reflected at coarse resolution (Punger and West, 2013). However, changes in $PM_{2.5}$ due to sulfate geoengineering are diffuse compared to modern anthropogenic $PM_{2.5}$, and this covariance is therefore likely to be reduced. These simulations also do not take into account the possible response of cloudiness to the increase in cloud condensation nuclei which could result from sulfate geoengineering, due to the descent of emitted fine aerosol into the upper troposphere. In addition to potentially affecting the total UV-B reaching the surface and the net RF associated with geoengineering (Kuebbeler et al., 2012), changes in cloudiness through this mechanism could affect surface precipitation and thereby $PM_{2.5}$ concentrations. Although outside the scope of this work, we consider assessment of the response of cloudiness to be a priority for future research on surface-level impacts of geoengineering.

These results must be weighed against the risks of climate change which sulfate geoengineering seeks to mitigate, and the magnitude of current and future health impacts due to degraded air quality. A study of the 2015 global burden of disease found that 4 million deaths annually are attributable to degraded air quality, while air quality co-benefits of greenhouse gas mitigation (including changes in precursor emissions) have been estimated at ∼1.3 million fewer mortalities per year in 2050 (Cohen et al., 2017; West et al., 2013). We find that the total air quality and skin cancer related impacts of sulfate geoengineering sufficient to induce a 1 °C decrease in surface temperature are +26,000 (95% CI: −30,000 to +79,000) premature mortalities per year. Normalizing by total population in 2040, this is equivalent to a change of +0.3 early deaths per 100,000 population. For context, this

Table 3
Annual premature mortality impacts resulting from sulfate geoengineering sufficient to offset 1 °C of surface warming. Mean outcomes are in bold, 95% intervals are shown in square brackets (N = 1000). The 95% interval is calculated as the 2.5 and 97.5th percentile values of the Monte Carlo simulation outcomes.

	Direct impacts		RF-driven impacts		
	Descending injection mass	Photochemical effects	Offset warming	Offset precipitation	All mechanisms
Surface ozone	-	**−23,000** (-45,000: 6600)	**−43,000** (-67,000: 19,000)	**−660** (-1100: 260)	**−67,000** (-110,000: 28,000)
$PM_{2.5}$	**7400** (2300: 16,000)	**−1400** (-2400: 520)	**69,000** (41,000: 95,000)	**14,000** (7100: 21,000)	**88,000** (53,000: 120,000)
UV-B	-	**4100** (1300: 8200)	**400** (200: 610)	**−24** (-40: 10)	**4500** (1600: 8800)
All causes	**7400** (2300: 16,000)	**−20,000** (-42,000: 4900)	**26,000** (-12,000: 63,000)	**13,000** (6600: 20,000)	**26,000** (-30,000: 79,000)

can be compared to projected direct health impacts of rising surface temperatures. A study of temperature-related mortality under a "business as usual" (BAU) climate change scenario projected that a 3 °C increase in average surface temperature would result in an additional 63,000 mortalities per year in the US alone, corresponding to +20 deaths per 100,000 population (Deschênes and Greenstone, 2011). These changes are dominated by increased vulnerability during extreme cold and extreme heat events, resulting in greater changes at higher baseline temperatures. Another study found that aggregate economic impacts of temperature increases are approximately linear in temperature, and that BAU climate change is estimated to reduce global average incomes by 23% within the next 80 years (Burke et al., 2015). These consequences of climate change must be weighed against the risks and benefits of sulfate geoengineering, including (but not limited to) the impacts on air quality and UV exposure explored in this study, which are relatively small and of uncertain sign.

5. Conclusions

We identify several mechanisms by which sulfate geoengineering may cause changes in air quality and UV-B exposure, and we provide the first quantitative estimates of the impact of sulfate geoengineering on global mortality rates from these causes. When sulfate geoengineering is used to offset 1 °C of temperature rise (or create 1 °C cooling) we find that RF-driven impacts, associated with offsetting the effects of climate change, result in a net increase in mortality, while other ("direct") impacts result in a net decrease. The net effect is an increase of 26,000 additional premature mortalities per year (95% interval: −30,000 to +79,000), although the overall sign of the impact is uncertain. We find an 83% chance of a net increase in global mortality due to air quality and UV-B exposure, with uncertainty in the exposure response functions providing the greatest contribution to total uncertainty in the result.

Of the direct impact pathways considered, descent of injected sulfate aerosol from the stratosphere is found to be a minor contributor to the overall impact of sulfate geoengineering. The contribution of descending, injected aerosol to surface $PM_{2.5}$ causes 7400 additional premature mortalities per year, compared to a decrease of 20,000 premature mortalities per year resulting from the direct photochemical effects of sulfate geoengineering. This is made up of 4100 additional skin cancer mortalities offset by 23,000 averted premature mortalities due to decreased ozone exposure. By contrast, RF-driven impacts of sulfate geoengineering are found to result in a net increase in mortality relative to the avoided future scenario. By offsetting 1 °C of atmospheric warming, greater concentrations of $PM_{2.5}$ are formed from existing emissions, resulting in an additional 69,000 premature mortalities per year. The reduction in radiative forcing also offsets some of the anticipated increase in precipitation associated with climate change, with longer aerosol lifetimes incurring an additional 14,000 premature mortalities per year. These effects are partially offset by 44,000 avoided mortalities per year from RF-driven changes in ozone exposure. The specific magnitudes depend on the amount of warming which is being offset. The impacts of larger or smaller amounts of can be approximated by scaling the warming to our 1 °C value.

This analysis does not account for ecological and climate feedback effects related to increased CO_2, possible induced or suppressed cloudiness, or public health impacts beyond changes in mortality due to air quality and UV-B exposure. Deschênes and Greenstone, 2011 found that, under a business-as-usual scenario with 3 °C of warming in 2070–2099, the direct impact of increased temperatures due to climate change would be 63,000 premature mortalities per year from extreme temperatures in the United States alone. Burke et al. (2015) estimated that aggregate economic impacts of climate change will reduce global average incomes by 23% in the same period. Although beyond the scope of this paper, weighing the broader effects of mitigating climate change against the air quality and UV-B impacts computed here would provide a more complete understanding of the net benefits and risks of sulfate geoengineering.

Appendix A. Assessment of response linearity

Four additional simulations are conducted to test the validity of the assumption that impacts will scale linearly with input. For impacts due to changes in temperature and precipitation, we simulate perturbations which are 5 times smaller than the CanESM2 output and 8.6 times smaller than the "full" perturbations corresponding to a 0.98 K cooling. A 0.5 TgS/yr injection rate, resulting in a 0.040 increase in stratospheric optical depth, was simulated to determine impact linearity with respect to these quantities in isolation from meteorological feedbacks. A full list is given in Table 4. Second order effects due to effect interaction (e.g. between precipitation impacts and injected sulfates) are addressed in Appendix B. The output metric shown is the total mortalities as calculated without accounting for uncertainty in climate or exposure response variables.

Table 4
Perturbation parameters used in simulations to establish response linearity.

Input	Small perturbation	Large perturbation
Injection rate (TgS/yr)	0.5	1.0
Optical depth ($-$)	0.040	0.079
Offset warming (K)	0.12	0.98
Offset precipitation (%)	0.28%	2.4%

The total mortalities calculated for each perturbation, broken down into those resulting from exposure to $PM_{2.5}$, ozone and UV-B, are shown in Fig. 3. Interpolation between zero and the 'full-scale' perturbation shows a good agreement with the results of the smaller test perturbation simulations. The exception to this is in the case of the response to an increase in stratospheric aerosol optical depth $\Delta\tau$. For a $\Delta\tau$ of 0.040, the change in mortality due to skin cancer is 21% greater than would be calculated by interpolation from the impact of a $\Delta\tau$ of 0.079, and the ozone reduction is 13% greater. The effect on $PM_{2.5}$ exposure is negligible. This is likely to be due to saturation, as reaction rates become limited by factors other than surface area density of aerosol.
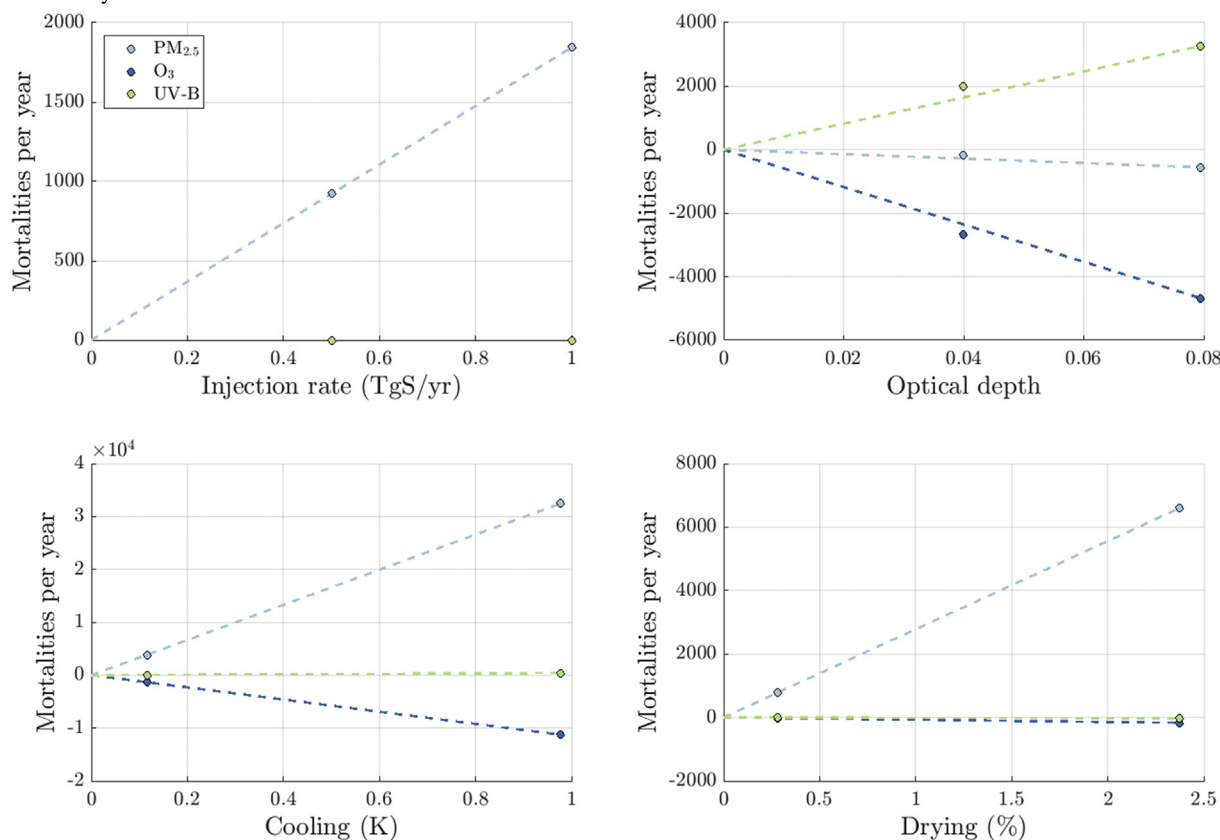
Fig. 3. Response linearity with respect to each of the assessed mortality mechanisms. The dashed line represents the linear sensitivity used in each case when scaling calculated exposures for the purposes of uncertainty quantification.

Appendix B. Second-order sensitivities

Four additional simulations are conducted in which the inputs are combined to determine the effect of second order terms on the response. In the first three simulations, combinations of two parameters (temperature change, precipitation change, and injection rate) are changed simultaneously. In the final simulation, all three are modified together. For these simulations, the effect of descending aerosol and the photochemical effect of an increase in stratospheric optical depth are not separated.

The results of these simulations are shown in Fig. 4. In each panel, the left-hand bar shows the total mortalities as calculated by linearly adding the exposure calculated by individual simulations, whereas the right-hand bar shows total mortalities as calculated using a single simulation in which the perturbations are simulated together. These estimates do not include uncertainty in climate variables. Inclusion of second-order effects changes the total calculated number of mortalities by less than ± 1%, suggesting that interaction between the three factors is not significant. However, this does not address possible meteorological feedbacks such as changes in cloud cover or ventilation.

Fig. 4. Comparison of mortalities estimated by linear combination of calculated exposures from several perturbation simulations (left) and by direct simulation of multiple perturbations together (right). All totals agree to within ± 1%. Uncertainty in climate variables is not included in these estimates.

Appendix A. Supplementary data

Supplementary data related to this article can be found at http://dx.doi.org/10.1016/j.atmosenv.2018.05.047.

References

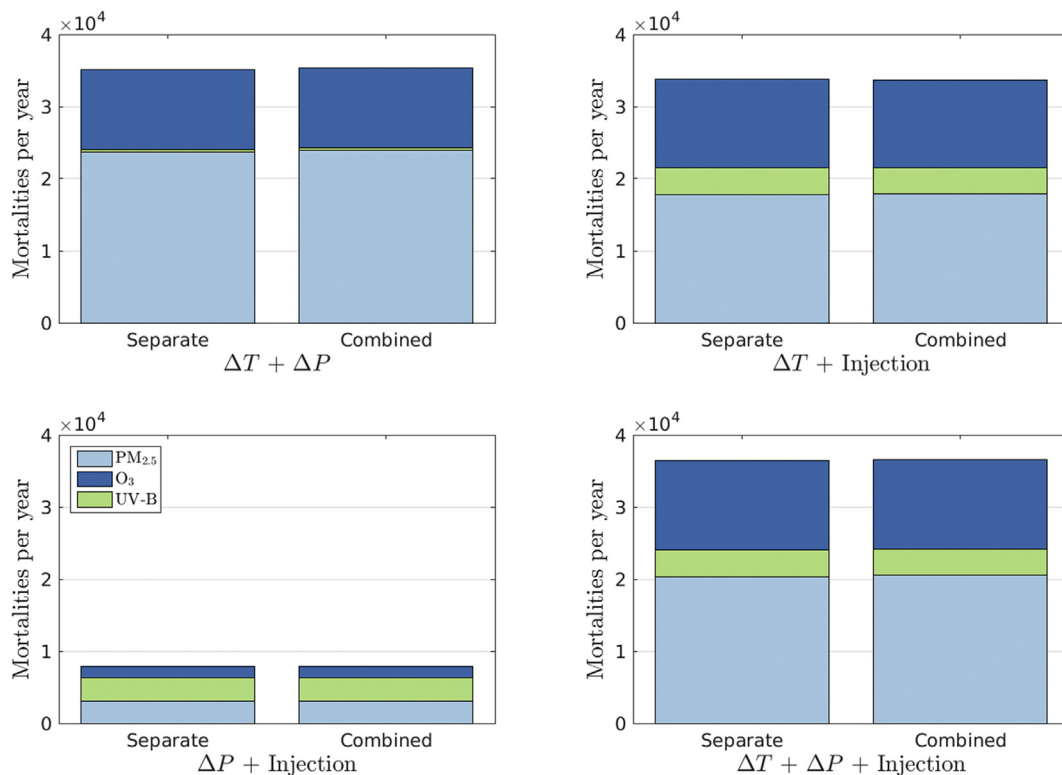Barrett, S.R.H., Yim, S.H.L., Gilmore, C.K., Murray, L.T., Kuhn, S.R., Tai, A.P.K., Yantosca, R.M., Byun, D.W., Li, X., Levy, J., Ashok, A., Koo, J., Wong, H.M., Dessens, O., Balasubramanian, S., Fleming, G.G., Malina, R., Pearlson, M.N., Arunachalam, S., Francis, S., 2012. Public health, climate and economic impacts of desulfurizing jet fuel. Environ. Sci. Technol. 46 (8), 4275–4282.

Benduhn, F., Schallock, J., Lawrence, M.G., 2016. Early growth dynamical implications for the steerability of stratospheric solar radiation management via sulfur aerosol particles. Geophys. Res. Lett. 43 (18), 2016GL070701.

Burke, M., Hsiang, S.M., Miguel, E., 2015. Global non-linear effect of temperature on economic production. Nature 1, 1–16.

Burnett, R.T., Pope, C.A., Ezzati, M., Olives, C., Lim, S.S., Mehta, S., Shin, H.H., Singh, G., Hubbell, B., Brauer, M., Anderson, H.R., Smith, K.R., Balmes, J.R., Bruce, N.G., Kan, H., Laden, F., Prüss-Ustün, A., Turner, M.C., Gapstur, S.M., Diver, W.R., Cohen, A., 2014. An integrated risk function for estimating the global burden of disease attributable to ambient fine particulate matter exposure. Environ. Health Perspect. 122, 397–403.

Caldeira, K., Bala, G., Cao, L., 2013. The science of geoengineering. Annu. Rev. Earth Planet Sci. 41 (1), 231–256.

Clarke, L., Edmonds, J., Jacoby, H., Pitcher, H., Reilly, J., Richels, R., 2007. Scenarios of Greenhouse Gas Emissions and Atmospheric Concentrations. Sub-report 2.1A of Synthesis and Assessment Product 2.1 by the U.S. Climate Change Science Program and the Subcommittee on Global Change Research Department of Energy, Office of Biological & Environmental Research, Washington.

Cohen, A.J., Brauer, M., Burnett, R., Anderson, H.R., Frostad, J., Estep, K., Balakrishnan, K., Brunekreef, B., Dandona, L., Dandona, R., Feigin, V., Freedman, G., Hubbell, B., Jobling, A., Kan, H., Knibbs, L., Liu, Y., Martin, R., Morawska, L., Pope 3rd, C.A., Shin, H., Straif, K., Shaddick, G., Thomas, M., van Dingenen, R., van Donkelaar, A., Vos, T., Murray, C.J.L., Forouzanfar, M.H., 2017. Estimates and 25-year trends of the global burden of disease attributable to ambient air pollution: an analysis of data from the Global Burden of Diseases Study 2015. Lancet 389, 1907–1918.

Corbett, J.J., Winebrake, J.J., Green, E.H., Kasibhatla, P., Eyring, V., Lauer, A., 2007. Mortality from ship emissions: a global assessment. Environ. Sci. Technol. 41 (24), 8512–8518.

de Gruijl, F.R., Van der Leun, J.C., 1994. Estimate of the wavelength dependency of ultraviolet carcinogenesis in humans and its relevance to the risk assessment of a stratospheric ozone depletion. Health Phys. 67, 319–325.

Deschênes, O., Greenstone, M., 2011. Climate change, mortality, and adaptation: evidence from annual fluctuations in weather in the U.S. Am. Econ. J. Appl. Econ. 3 (4), 152–185.

Eastham, S.D., Barrett, S.R.H., 2016. Aviation-attributable ozone as a driver for changes in mortality related to air quality and skin cancer. Atmos. Environ. 144, 17–23.

Eastham, S.D., Weisenstein, D.K., Barrett, S.R.H., 2014. Development and evaluation of the unified tropospheric–stratospheric chemistry extension (UCX) for the global chemistry-transport model GEOS-Chem. Atmos. Environ. 89, 52–63.

Effiong, U., Neitzel, R.L., 2016. Assessing the direct occupational and public health impacts of solar radiation management with stratospheric aerosols. Environ. Health 15 (1), 7.

Fiore, A.M., Naik, V., Spracklen, D.V., Steiner, A., Unger, N., Prather, M., Bergmann, D., Cameron-Smith, P.J., Cionni, I., Collins, W.J., Dalsøren, S., Eyring, V., Folberth, G.A., Ginoux, P., Horowitz, L.W., Josse, B., Lamarque, J.-F., MacKenzie, I.A., Nagashima, T., O'Connor, F.M., Righi, M., Rumbold, S.T., Shindell, D.T., Skeie, R.B., Sudo, K., Szopa, S., Takemura, T., Zeng, G., 2012. Global air quality and climate. Chem. Soc. Rev. 41, 6663.

Guy, G.P., Machlin, S.R., Ekwueme, D.U., Yabroff, K.R., 2015. Prevalence and costs of skin cancer treatment in the u.s., 2002-2006 and 2007-2011. Am. J. Prev. Med. 48 (2), 183–187.

Heckendorn, P., Weisenstein, D., Fueglistaler, S., Luo, B.P., Rozanov, E., Schraner, M., Thomason, L.W., Peter, T., 2009. The impact of geoengineering aerosols on stratospheric temperature and ozone. Environ. Res. Lett. 4 (4), 045108.

Hoek, G., Krishnan, R.M., Beelen, R., Peters, A., Ostro, B., Brunekreef, B., Kaufman, J.D., 2013. Long-term air pollution exposure and cardio- respiratory mortality: a review. Environ. Health 12 (1), 43.

Jerrett, M., Burnett, R.T., Pope, C.A., Ito, K., Thurston, G., Krewski, D., Shi, Y., Calle, E., Thun, M., 2009. Long-term ozone exposure and mortality. N. Engl. J. Med. 360 (11), 1085–1095.

Kirtman, B., Power, S.B., Adedoyin, J.A., Boer, G.J., Bojariu, R., Camilloni, I., Doblas-Reyes, F.J., Fiore, A.M., Kimoto, M., Meehl, G.A., Prather, M., Sarr, A., Schär, C., Sutton, R., van Oldenborgh, G.J., Vecchi, G., Wang, H.J., 2014. Near-term climate change: projections and predictability. In: Stocker, T.F., Qin, D., Plattner, G.-K., Tignor, M., Allen, S.K., Boschung, J., Nauels, A., Xia, Y., Bex, V., Midgley, P.M. (Eds.), Climate Change 2013: the Physical Science Basis. Contribution of Working Group I to the Fifth Assessment Report of the Intergovernmental Panel on Climate Change. Cambridge University Press, Cambridge, pp. 953–1028.

Kravitz, B., Robock, A., Forster, P.M., Haywood, J.M., Lawrence, M.G., Schmidt, H., 2013. An overview of the geoengineering model intercomparison project (GeoMIP). J. Geophys. Res. Atmos. 118 (23), 13,103–113,107.

Kravitz, B., MacMartin, D.G., Robock, A., Rasch, P.J., Ricke, K.L., Cole, J.N.S., Curry, C.L., Irvine, P.J., Ji, D., Keith, D.W., Egill Kristjánsson, J., Moore, J.C., Muri, H., Singh, B., Tilmes, S., Watanabe, S., Yang, S., Yoon, J.-H., 2014. A multi-model assessment of regional climate disparities caused by solar geoengineering. Environ. Res. Lett. 9. https://doi.org/10.1088/1748-9326/9/7/074013.

Krewski, D., Jerrett, M., Burnett, R.T., Ma, R., Hughes, E., Shi, Y., Turner, M.C., Pope, C.A.I., Thurston, G., Calle, E.E., Thun, M.J., 2009. Extended Follow-up and Spatial Analysis of the American Cancer Society Study Linking Particulate Air Pollution and Mortality. HEI Research Report 140. Health Effects Institute, Boston, MA.

Kuebbeler, M., Lohmann, U., Feichter, J., 2012. Effects of stratospheric sulfate aerosol geo-engineering on cirrus clouds. Geophys. Res. Lett. 39.

Li, F., Stolarski, R.S., Newman, P.A., 2009. Stratospheric ozone in the post-CFC era. Atmos. Chem. Phys. 9, 2207–2213.

McCormick, M.P., Thomason, L.W., Trepte, C.R., 1995. Atmospheric effects of the Mt Pinatubo eruption. Nature 373, 399–404.

United States National Academy of Sciences (NAS) Geoengineering, 1992. In Policy Implications of Greenhouse Warming: Mitigation, Adaptation, and the Science Base.

Niemeier, U., Timmreck, C., 2015. What is the limit of climate engineering by stratospheric injection of SO_2? Atmos. Chem. Phys. 15 (16), 9129–9141.

Nowack, P.J., Abraham, N.L., Braesicke, P., Pyle, J.A., 2016. Stratospheric ozone changes under solar geoengineering : implications for UV exposure and air quality. Atmos. Chem. Phys. 16, 4191–4203.

Pierce, J.R., Weisenstein, D.K., Heckendorn, P., Peter, T., Keith, D.W., 2010. Efficient formation of stratospheric aerosol for climate engineering by emission of condensible vapor from aircraft. Geophys. Res. Lett. 37 (18). http://dx.doi.org/10.1029/2010GL043975.

Pitari, G., Aquila, V., Kravitz, B., 2014. Stratospheric ozone response to sulfate geoengineering: results from the geoengineering model intercomparison project (GeoMIP). Geophys. Res. Atmos. 2629–2653 (November 1991).

Punger, E.M., West, J.J., 2013. The effect of grid resolution on estimates of the burden of ozone and fine particulate matter on premature mortality in the USA. Air Qual. Atmos. Health 6 (3), 563–573.

Rasch, P.J., Crutzen, P.J., Coleman, D.B., 2008. Exploring the geoengineering of climate using stratospheric sulfate aerosols: the role of particle size. Geophys. Res. Lett. 35

(2), 1–6.

Reilly, J., Hohmann, N., Kane, S., 1994. Climate change and agricultural trade: who benefits, who loses? Global Environ. Change 4, 24–36.

Saltelli, A., Ratto, M., Andres, T., Campolongo, F., Cariboni, J., Gatelli, D., Saisana, M., Tarantola, S., 2008. Global Sensitivity Analysis: the Primer. Wiley.

Slaper, H., Velders, G.J., Daniel, J.S., de Gruijl, F.R., van der Leun, J.C., 1996. Estimates of ozone depletion and skin cancer incidence to examine the Vienna Convention achievements. Nature 384 (6606), 256–258.

Smith, S.J., Wigley, T.M.L., 2006. Multi-gas forcing stabilization with MiniCAM. Energy J. (Special Issue #3), 373–391.

Smith, S.J., van Aardenne, J., Klimont, Z., Andres, R.J., Volke, A., Delgado Arias, S., 2011. Anthropogenic sulfur dioxide emissions: 1850–2005. Atmos. Chem. Phys. 11, 1101–1116.

Tilmes, S., Garcia, R.R., Kinnison, D.E., Gettelman, A., Rasch, P.J., 2009. Impact of geoengineered aerosols on the troposphere and stratosphere. J. Geophys. Res. 114 (D12), D12305.

Tilmes, S., Kinnison, D.E., Garcia, R.R., Salawitch, R., Canty, T., Lee-Taylor, J., Madronich, S., Chance, K., 2012. Impact of very short-lived halogens on stratospheric ozone abundance and UV radiation in a geo-engineered atmosphere. Atmos. Chem. Phys. 12, 10945–10955.

United Nations Department of Economic and Social Affairs (Population Division), 2013. World Population Prospects: the 2012 Revision.

Weisenstein, D.K., Yue, G.K., Ko, M.K.W., Sze, N.-D., Rodriguez, J.M., Scott, C.J., 1997. A two-dimensional model of sulfur species and aerosols. J. Geophys. Res. 102 (97).

Weisenstein, D.K., Penner, J.E., Herzog, M., Liu, X., 2007. Global 2-D intercomparison of sectional and modal aerosol modules. Atmos. Chem. Phys. 7, 2339–2355.

West, J.J., Smith, S.J., Silva, R.A., Naik, V., Zhang, Y., Adelman, Z., Fry, M.M., Anenberg, S., Horowitz, L.W., Lamarque, J.-F., 2013. Co-benefits of global greenhouse gas mitigation for future air quality and human health. Nat. Clim. Change 3, 885–889.

Wise, M., Calvin, K., Thomson, A., Clarke, L., Bond-Lamberty, B., Sands, R., Smith, S.J., Janetos, A., Edmonds, J., 2009. Implications of limiting CO2 concentrations for land use and energy. Science 324 (5931), 1183–1186.

Xia, L., Nowack, P.J., Tilmes, S., Robock, A., 2017. Impacts of stratospheric sulfate geoengineering on tropospheric ozone. Atmos. Chem. Phys. 17 (19), 11913–11928.

Zhang, H., Wu, S., Huang, Y., Wang, Y., 2014. Effects of stratospheric ozone recovery on photochemistry and ozone air quality in the troposphere. Atmos. Chem. Phys. 14, 4079–4086.